Joint Mismatch and Channel Compensation for High-Speed OFDM Receivers with Time-Interleaved ADCs

Sandeep Ponnuru, Munkyo Seo, Upamanyu Madhow, *Fellow, IEEE*, and Mark Rodwell, *Fellow, IEEE*

***Abstract*—Analog-to-digital converters (ADCs) with high sampling rates and output resolution are required for the design of mostly digital transceivers in emerging multi-Gigabit communication systems. A promising approach is to use a time-interleaved (TI) architecture with slower sub-ADCs in parallel, but mismatch among the sub-ADCs, if left uncompensated, can cause error floors in receiver performance. Conventional mismatch compensation schemes typically have complexity (in terms of number of multiplications) that increases with the desired resolution at the output of the TI-ADC. In this paper, we investigate an alternative approach, in which mismatch and channel dispersion are compensated jointly, with the performance metric being overall link reliability rather than ADC performance. For an OFDM system, we characterize the structure of mismatch-induced interference, and demonstrate the efficacy of a frequency-domain interference suppression scheme whose complexity is independent of constellation size (which determines the desired resolution). Numerical results from computer simulation and from experiments on a hardware prototype show that the performance with the proposed joint mismatch and channel compensation technique is close to that without mismatch. While the proposed technique works with offline estimates of mismatch parameters, we provide an iterative, online method for joint estimation of mismatch and channel parameters which leverages the training overhead already available in communication signals.**

***Index Terms*—Multi-gigabit, analog-to-digital converter, time-interleaved A/D converter, OFDM, mismatch.**

I. Introduction

MOSTLY digital transceiver architectures have been key to the economies of scale for cellular and wireless local area networks. By deriving most of its functionality from a digital-signal processor (DSP) core, a mostly digital transceiver can exploit "Moore's law", or the exponential downscaling of the per transistor size to realize fast, low-cost hardware for the transceiver [1]. However, a major bottleneck in extending this advantage to future multi-Gigabit systems is that the analog-to-digital converters (ADCs) required prior to the baseband DSP core are either unavailable, or are too costly and power hungry [2]. For example, systems operating over the 3.1-10.6 GHz band [28] or the unlicensed 60 GHz band (57-64 GHz in US) [29] require ADCs with sampling rates of the order of GHz. Furthermore, mostly digital receiver processing for large constellations, dispersive channels, or multiple antennas requires relatively high resolution (e.g., 6-10 bits). The Flash ADC [2] is conventionally the architecture of choice for high sampling rates, but its power consumption scales exponentially with resolution, and it is difficult to obtain more than 5-6 bits of resolution at multi-GHz sampling rates. In this paper, we explore time-interleaved (TI) ADCs, which provide an attractive alternative for achieving both high speed and high resolution at reasonable power consumption. The idea is to use power-efficient ADC architectures, such as the pipelined or the successive approximation architecture, to obtain high-resolution ADCs at relatively low speeds (e.g., 50 MHz in [3], [4]), and to use them in parallel to synthesize a high-rate ADC, as shown in Fig. 1. We refer to each constituent low-rate ADC as a *sub-ADC*.

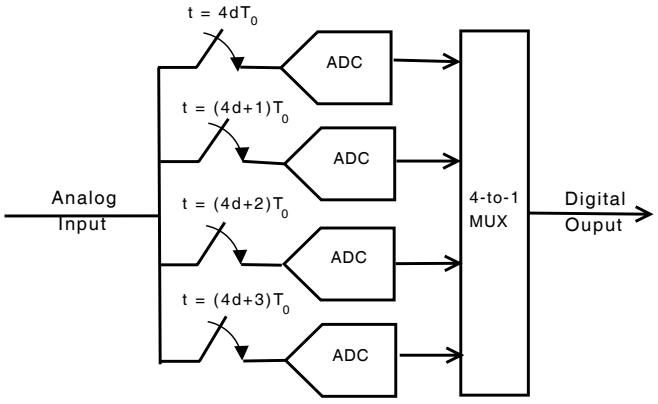

Fig. 1. A time-interleaved ADC formed by interleaving four sub-ADCs (d = integer, T_o = sampling period).

A major bottleneck in realizing a TI-ADC is mismatch among the sub-ADCs; Fig. 2 depicts, for example, mismatches in gain, timing and voltage offset. Causes of mismatch include imperfect clock distribution, variation of transistor size, signal path differences, and parasitic effects. Mismatch compensation for general-purpose TI-ADCs has received significant attention [5]. In this paper, we ask whether there are simpler alternatives to the standard techniques of explicit mismatch estimation and compensation for the specific application to communication receivers.

Paper approved by M. Juntti, the Editor for MIMO and Multiple-Access of the IEEE Communications Society. Manuscript received November 13, 2009; revised February 10, 2010.

This work was supported in part by the National Science Foundation under grant CCF-0729222. This paper was presented in part at the IEEE Global Communications Conference (GLOBECOM) held at New Orleans, USA, Dec. 2008.

S. Ponnuru, U. Madhow, and M. Rodwell are with the Department of Electrical and Computer Engineering, University of California, Santa Barbara CA 93106, USA (e-mail: sandeep_ponnuru@umail.ucsb.edu, {madhow, rodwell}@ece.ucsb.edu).

M. Seo is with Teledyne Scientific Company, 1049 Camino Dos Rios, Thousand Oaks, CA 91360, USA (e-mail: mkseo@ieee.org).

Digital Object Identifier 10.1109/TCOMM.2010.08.090693

A. Contributions

Our approach differs from conventional TI-ADC mismatch compensation, in that the TI-ADC is viewed as part of the overall communication link, and our goal is to jointly compensate for mismatch and channel dispersion. Our performance metric is overall link reliability rather than the performance of the ADC as an isolated component, with the main goal being to simplify the task of mismatch compensation. In addition, our approach, while being compatible with offline mismatch estimation, offers the advantage that it becomes possible to leverage the training inherent in communication signals for online mismatch estimation.

We illustrate our ideas for an orthogonal frequency division multiplexing (OFDM) receiver, where the TI-ADCs employed may have gain, timing and voltage offset mismatches among the sub-ADCs. Our main contributions are as follows:

- Since we are interested in demodulating constellation points in the frequency domain, we model the effect of mismatch in the frequency domain, after the discrete Fourier transform performed by the OFDM receiver. The interference due to voltage offset mismatch is signal-independent, but the interference due to gain and timing mismatch is signal-dependent, and is shown to cause inter-subcarrier interference between nominally orthogonal OFDM subcarriers. If left uncompensated, this leads to an error floor in the bit error rate (BER), which we quantify through numerical experiments.
- For the special case when the number of sub-ADCs divides the number of subcarriers, the subcarriers form *interference groups,* such that only subcarriers within a group interfere with each other. This reduces the complexity of interference suppression, since the size of the interference group is at most $2L$, where L denotes the number of the sub-ADCs in each of the TI-ADCs employed for sampling the in-phase (I) and quadrature-phase (Q) channels.
- We show that zero-forcing interference suppression within an interference group, which requires $4L$ real-valued coefficients, is effective for joint mismatch compensation and demodulation, regardless of the desired resolution (the latter depends on the size of the constellations we wish to support). In contrast, the complexity (in terms of the number of multiplications) of the conventional time-domain mismatch compensation for TI-ADCs increases with the desired resolution.
- We show that it is possible to estimate mismatch and channel parameters jointly using an iterative technique, using training sequences provided for channel estimation. This involves estimating mismatch parameters and channel parameters alternately. Simulation results show that a near-optimal solution is obtained in as few as three iterations for the examples considered. These estimates are shown to be effective when plugged into our joint mismatch compensation and demodulation scheme, yielding a performance that is close to that without mismatch.
- We report on results from an experimental prototype built by interleaving four commercially available ADCs, each sampling at 100 MSa/s with 14 bits of nominal resolution. (The ADC parameters for the prototype are dictated by what was easily available off-the-shelf; for the multiGigabit applications that motivate this paper, integrated circuit realizations of the sub-ADCs would probably employ higher sampling rates and have lower resolution). The resultant TI-ADC is fed with a typical OFDM received (baseband) signal. The mismatches in the assembled ADC are estimated using the proposed iterative algorithm and compensated jointly with the demodulation. The experimental results demonstrate the efficacy of the proposed mismatch and channel compensation technique, and show excellent agreement with theoretical predictions.

Example application: The proposed approach is most attractive when the number of sub-ADCs (and hence the size of the interference group) is moderate. For example, consider a mostly digital receiver for a multi-Gigabit system operating in the mm-wave band [29]. For 16-QAM modulation on each subcarrier, OFDM transmission (with no excess bandwidth) using 1 GHz of the spectrum results in a raw bit rate of 4 Gbps. Numerical results indicate that the two TI-ADCs (each sampling at a rate of 1 GHz), one for each of the I and Q channels, should have a minimum of 8 bits of resolution for the digital output. When we use a time-interleaved architecture with eight sub-ADCs, the sampling rate is 125 MHz for each sub-ADC, which is slow enough that we can use power efficient successive-approximation or pipelined architectures to implement the sub-ADCs [3], [4]. The complexity of the frequency-domain equalizer (32 real-valued multiplications per sample) is independent of the resolution: we can increase sub-ADC resolution as we scale up the constellation (e.g., to 256-QAM, instead of the 16-QAM constellation considered in our examples here), but the complexity of the zero-forcing equalizer would remain the same.

B. Prior work

The time-interleaving architecture has attracted much attention [6]-[27] due to its potential for realizing high-speed, high-resolution converters with reduced power dissipation. A number of mismatch models have been proposed, ranging from simpler models including gain, timing and voltage offset mismatches, to more general models of mismatched frequency responses [11], [12], [15], [17].

Some recently proposed designs use efficient clocking schemes and redundant elements as a means of overcoming mismatch [6], [7], [8]. The scalability of such approaches to higher speeds and resolution requires further investigation. Other than these references, prior approaches typically consist of first estimating the mismatch parameters, and then compensating the output of the ADC.

Mismatch estimation: Mismatch estimation can be performed blindly by comparing the statistics of the digital output between the mismatched and the ideal TI-ADCs [14], [17], [18], [19]. However, reliable blind estimation needs a large sample size. Training-based schemes are faster, but for general-purpose ADCs where the input can be arbitrary, they require the additional expense of separate hardware for test sequence generation [13], [15].

Mismatch compensation: Once the mismatch parameters are estimated, the compensation scheme depends on the type of mismatch. Voltage-offset and gain mismatches can be compensated using a simple subtraction and scalar gain respectively. On the other hand, timing mismatch, or more generally, frequency response mismatches, need a set of parallel finite-impulse response (FIR) filters for compensation [15]-[23]. In addition to such digital compensation schemes, a number of analog techniques have also been proposed [13], [14].

As already discussed, our approach differs from the literature in two respects: we compensate for mismatch and channel dispersion jointly, and we are able to leverage the training overhead in communication for the estimation of mismatch parameters. We note that there have indeed been prior attempts in utilizing communication training sequences for mismatch compensation [24], but these are restricted to estimating and subtracting the signal-independent interference due to voltage offset mismatch. Prior work on characterizing the effect of gain, timing and voltage offset mismatches on a singlecarrier communication system includes [25].

A radically different approach to overcome the ADC bottleneck at high sampling rates is to use an extremely low resolution ADC (1-4 bits). But this introduces a significant non-linearity at the start of the receiver and hence, demands a complete redesign of the entire transceiver [26], [27]. While such an approach might be appropriate for some applications (e.g., a small constellation used over a line-of-sight channel), the TI-ADC approach is applicable more generally, especially to settings that require a larger dynamic range.

C. Notation

Bold-faced symbols are used for vectors and matrices. For example, an $M \times 1$ column vector $\boldsymbol{X}$ equals $(X[0], \cdots, X[M-1])^t$, where the superscript t denotes transpose. We use the notation $\boldsymbol{X}^*$ to represent a vector/matrix obtained by taking the complex conjugates of all the individual elements in $\boldsymbol{X}$. We use $\Re[\cdot]$ and $\Im[\cdot]$ to represent the real and imaginary parts of a vector/matrix. The concatenation of the real and imaginary parts of a vector $\boldsymbol{X}$, that is the vector $(\Re[\boldsymbol{X}]^t \quad \Im[\boldsymbol{X}]^t)^t$, is denoted by $\tilde{\boldsymbol{X}}$.

D. Organization

In Section II, we describe the system model, including the TI-ADC with mismatch, and the OFDM transceiver. The mismatch-induced interference is characterized in Section III, and our proposed frequency-domain joint mismatch compensation and demodulation scheme is described in Section IV. An iterative scheme for mismatch and channel estimation is presented in Section V. Numerical results from simulation and hardware experiments are presented in Section VI, while Section VII contains our conclusions.

II. System Model

In this section, we first give a model for the TI-ADC with gain, timing and voltage offset mismatches. Next, we give details about the received signal in OFDM transmission, which would serve as the analog input for the TI-ADC.

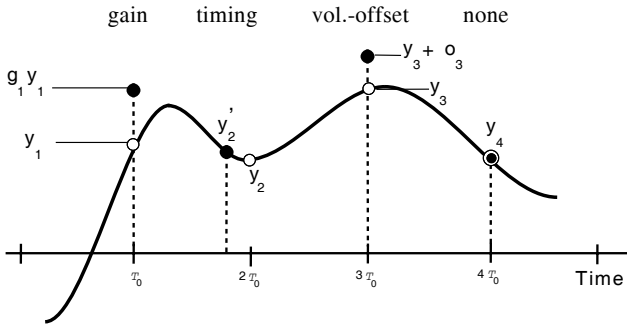

Fig. 2. Effect of TI-ADC mismatch on the sampling of the input analog signal: the four consecutive samples (from left to right) experience gain, timing, voltage offset and no mismatches respectively. The samples obtained by the TI-ADC with mismatches, indicated by •, are compared with the "○" samples; the latter being obtained when there are no mismatches.

A. TI-ADC Mismatch Model

In Fig. 2, we illustrate the effect of mismatch on the sampling of the input analog signal $r(t)$. Gain and voltage offset mismatches result in memoryless effects on the ideal samples (simple multiplicative and additive effects, respectively). On the other hand, the effect of timing mismatch depends on the actual signal (or specifically, on the values it takes between the ideal sampling instants). Letting $\frac{1}{T_o}$ denote the *nominal sampling rate*, the output of the TI-ADC can be written as [11]

$$r[m] = (1 + g_{m \bmod L}) r((m + \delta_{m \bmod L}) T_o) + \mu_{m \bmod L} \quad (1)$$

where $r[m]$ denotes the m^{th} sample, sampled by the sub-ADC with index $m \bmod L$, where L denotes the number of sub-ADCs and mod denotes the modulo operation. The gain, timing and voltage offset mismatches of the sub-ADC with index $m \bmod L$ are denoted by $g_{m \bmod L}$, $\delta_{m \bmod L}$, and $\mu_{m \bmod L}$ respectively, where the timing mismatches $\delta_{m \bmod L}$ have been normalized with respect to T_o. In the settings of interest to us [15], [16], [21] mismatch-induced interference and receiver thermal noise dominate quantization noise (which is small for a moderately high sub-ADC resolution), hence we neglect the latter from our analysis. Since drift in mismatch parameters occurs over durations of hours, we can neglect it in our framework. We therefore model the mismatch parameters as constant between successive training phases. In what follows, we omit explicitly writing "mod L" in the subscripts in order to simplify notation.

B. OFDM Model

We briefly review the standard OFDM transceiver operating over a dispersive channel, as shown in Fig. 3 [30]. Information-bearing symbols (drawn from a constellation such as QPSK) are encoded onto M subcarriers by using the inverse of the Fast Fourier transform (IFFT) operation (of size M) at the transmitter. The IFFT output (M time-domain symbols) constitutes one OFDM frame, and a cyclic prefix is conventionally added before each frame to convert the linear convolution between the communication channel and the time-domain symbols into a circular one. This converts the vector channel equalization to a scalar problem. After downconversion, the receiver performs FFT on the Nyquist-sampled received baseband signal, and then performs scalar

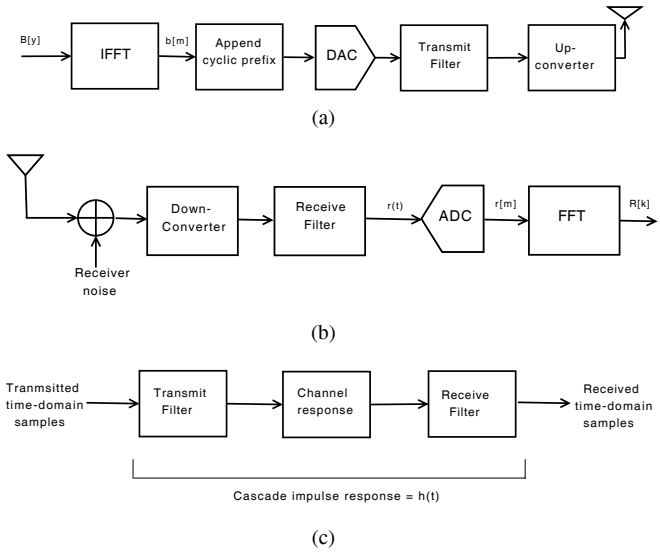

Fig. 3. (a) OFDM Transmitter (DAC = Digital-to-Analog Converter) (b) OFDM Receiver (c) Baseband signal model (time-domain)

equalization and demodulation of the constellation symbols separately for each subcarrier.

We denote the Nyquist sample period by T, so that the baseband signal (assuming no excess bandwidth) occupies the band $\left[-\frac{1}{2T}, \frac{1}{2T}\right]$. To simplify notation, we use the band $\left[0, \frac{1}{T}\right]$ for analysis. We refer to this as the *signal* band. The transmit and receive filters in Fig. 3 are assumed to be ideal lowpass filters in the signal band. The receiver input noise, $w(t)$, is assumed to be proper, complex, zero-mean, white, Gaussian process with a power spectral density N_o. The noise at the output of the receive-filter, $n(t)$, follows the same statistics but with a non-zero power spectral density (equal to N_o) only in the signal band. The impulse response of the cascade of the transmitter, channel and receive filters is denoted by $h(t)$. We assume that $h(t)$ is zero outside $[0, NT]$, where $N \ll M$ is a measure of the delay-spread of the communication channel. The length of the cyclic prefix (in Nyquist rate samples) should be at least N, in order to maintain the orthogonality of the subcarriers after the FFT.

III. The Structure of Mismatch-Induced Interference

Assuming a long enough cyclic prefix, we ignore the effect of samples from adjacent frames on the current OFDM frame, and consider an isolated frame for analysis. The input to the TI-ADC is then given in terms of time-domain symbols $\{b[m]\}$ as

$$r(t) = \sum_{m=-N}^{M-1} b[m \bmod M] h(t - mT) + n(t) \qquad (2)$$

Since the information-bearing symbols are encoded onto frequency domain subcarriers, we rewrite the time-domain symbols $\{b[m]\}$ in terms of the frequency domain symbols $\{B[y]\}$ (which are related by the energy-preserving FFT operation):

$$r(t) = \frac{1}{\sqrt{M}} \sum_{y=0}^{M-1} B[y] \sum_{m=-N}^{M-1} h(t-mT) e^{j2\pi y m/M} + n(t) \quad (3)$$

Since $h(t) \approx 0$ outside $[0, NT]$, all the significant samples of h (at rate T^{-1}) lie in $[0, NT]$, and it can be readily observed from (3) that the summation over m accounts for all these significant samples, as long as t is restricted to lie in $[0, (M-1)T]$. Hence, we can convert the finite summation over m in (3) to an infinite summation,

$$r(t) = \sum_{y=0}^{M-1} B[y] \phi_y(t) \sum_{m=-\infty}^{\infty} h(t - mT) e^{-\frac{j2\pi y}{MT}(t-mT)} + n(t) \qquad (4)$$

where $\phi_y(t) = \frac{1}{\sqrt{M}} e^{\frac{j2\pi y t}{MT}}$. Let $H(f)$ denote the Fourier transform of $h(t)$. Since the transmit filter is bandlimited to the signal band, $H(f)$ is also bandlimited, hence we can apply the Poisson's summation formula for the summation over m in (4) to obtain,

$$r(t) = \sum_{y=0}^{M-1} H[y] B[y] \phi_y(t) + n(t) \qquad (5)$$

where $H[y] = \frac{1}{MT} H\left(\frac{y}{MT}\right)$ or alternately, $\{H[y]\}$ are related to the sequence of the symbol-rate channel taps in the time-domain, $\{h[m] = h(mT)\}$, by the discrete Fourier transform of size M. We can rewrite the signal part of (5) in terms of the In-Phase (I) and Quadrature-Phase (Q) components as follows:

$$r(t) = \sum_{y=0}^{M-1} \Re[S[y]\phi_y(t)] + j \sum_{y=0}^{M-1} \Im[S[y]\phi_y(t)] \qquad (6)$$

where $S[y] = H[y]B[y]$. Now, we perform Nyquist rate sampling of I and Q waveforms using two different TI-ADCs with mismatch parameter sets $\{(g_{I,m}, \delta_{I,m}, \mu_{I,m})\}$ and $\{(g_{Q,m}, \delta_{Q,m}, \mu_{Q,m})\}$ respectively. Using (1) in (6) with $T_o = T$, the ordered pair of the samples of I and Q components is given as,

$$r_I[m] = \frac{(1+g_{I,m})}{\sqrt{M}} \sum_{y=0}^{M-1} \Re\left[S[y] e^{\frac{j2\pi y(m+\delta_{I,m})}{M}}\right] + \mu_{I,m}$$
$$r_Q[m] = \frac{(1+g_{Q,m})}{\sqrt{M}} \sum_{y=0}^{M-1} \Im\left[S[y] e^{\frac{j2\pi y(m+\delta_{Q,m})}{M}}\right] + \mu_{Q,m} \qquad (7)$$

We now obtain the complex-valued samples $\boldsymbol{r} = \{r_I[m] + j r_Q[m]\}$ as

$$\boldsymbol{r} = \frac{1}{2\sqrt{M}} \left[(\boldsymbol{\Delta}_I + \boldsymbol{\Delta}_Q)\boldsymbol{S} + (\boldsymbol{\Delta}_I^* - \boldsymbol{\Delta}_Q^*)\boldsymbol{S}^*\right] + \boldsymbol{\mu}, \qquad (8)$$

where $\boldsymbol{\mu} = \{\mu_{I,m} + j\mu_{Q,m}\}$, and we have $\boldsymbol{S} = \{S[y]\}$ following the bold-faced notation in Section I-C. The $(m,y)^{\text{th}}$ element of the matrix $\boldsymbol{\Delta}_I$ (and $\boldsymbol{\Delta}_Q$) is given as

$$\begin{aligned} \boldsymbol{\Delta}_I(m,y) &= (1+g_{I,m}) e^{\frac{j2\pi y}{M}(m+\delta_{I,m})} \\ \boldsymbol{\Delta}_Q(m,y) &= (1+g_{Q,m}) e^{\frac{j2\pi y}{M}(m+\delta_{Q,m})} \end{aligned} \qquad (9)$$

In (9), the indices m and y take integer values between 0 and $M-1$. We now take the (energy-preserving) FFT of the complex samples $\boldsymbol{r}$ in (8) to obtain

$$\boldsymbol{R} = \frac{1}{2M} \left[\boldsymbol{F}(\boldsymbol{\Delta}_I + \boldsymbol{\Delta}_Q)\boldsymbol{S} + \boldsymbol{F}(\boldsymbol{\Delta}_I^* - \boldsymbol{\Delta}_Q^*)\boldsymbol{S}^*\right] + \boldsymbol{\Upsilon} \quad (10)$$

where $\boldsymbol{F}$ denotes the standard FFT matrix of size M, and the vectors $\boldsymbol{R}$ and $\boldsymbol{\Upsilon}$ represent the (energy-preserving) FFT of the vectors $\boldsymbol{r}$ and $\boldsymbol{\mu}$ respectively.

It is worth checking that the model in (10) reduces to an OFDM system with no mismatch by setting $\boldsymbol{\Delta}_I = \boldsymbol{\Delta}_Q = \boldsymbol{F}^*$ and $\boldsymbol{\Upsilon} = 0$. This gives $\boldsymbol{R} = \boldsymbol{S}$, since the product $\boldsymbol{F}\boldsymbol{F}^*$ equals M times the identity matrix. Estimates for the information-bearing symbols $\boldsymbol{B}$ can be obtained by correlating with the corresponding channel gains, followed by the demodulation of constellation symbols.

With mismatch, however, the model for $\boldsymbol{R}$ is more complicated, and we observe from (10) the effect of different types of mismatch. Voltage offset mismatch adds signal-independent interference to the subcarriers, and can be compensated by simple subtraction. Gain and timing mismatches cause inter-subcarrier interference, and require an equalizer for compensation. A simpler approach to compensate gain mismatch is to apply time-varying gains to the time domain samples in (7), but timing mismatch cannot be compensated for in such a simple fashion in either the time or frequency domain, and requires an equalizer. We combine the tasks of gain and timing mismatch compensation, since the complexity is not reduced by addressing gain mismatch separately.

IV. Frequency domain Joint Mismatch Compensation and Demodulation

In this section, we design zero-forcing equalizers to compensate for the signal-dependent interference induced by the gain and timing mismatches following the model given in (10). Towards the end of the section, we provide a heuristic argument that indicates that the noise enhancement from such a scheme should be minimal. Since the equalizer operates on the FFT outputs $\boldsymbol{R}$, we refer to it as a *frequency-domain* zero-forcing equalizer.

For the model in (10), we first note that $\boldsymbol{S}$ and $\boldsymbol{S}^*$ are dependent. In order to formulate an unconstrained problem, we rewrite (10) in terms of the real and imaginary components of $\boldsymbol{S}$ as

$$\tilde{\boldsymbol{R}} = \boldsymbol{A}\tilde{\boldsymbol{S}} + \tilde{\boldsymbol{\Upsilon}} \tag{11}$$

The matrix $\boldsymbol{A}$ in (11) is defined as

$$\boldsymbol{A} := \tilde{\boldsymbol{F}}\tilde{\boldsymbol{\Delta}}, \qquad \text{where } \tilde{\boldsymbol{F}} = \begin{pmatrix} \Re[\boldsymbol{F}] & -\Im[\boldsymbol{F}] \\ \Im[\boldsymbol{F}] & \Re[\boldsymbol{F}] \end{pmatrix} \text{ and } \tilde{\boldsymbol{\Delta}} = \begin{pmatrix} \Re[\boldsymbol{\Delta}_I] & -\Im[\boldsymbol{\Delta}_I] \\ \Im[\boldsymbol{\Delta}_Q] & \Re[\boldsymbol{\Delta}_Q] \end{pmatrix} \tag{12}$$

If the matrix $\boldsymbol{A}$ is invertible, we obtain a zero-forcing equalizer for $\tilde{\boldsymbol{S}}$ as follows:

$$\tilde{\boldsymbol{S}} = \boldsymbol{A}^{-1}(\tilde{\boldsymbol{R}} - \tilde{\boldsymbol{\Upsilon}}) \tag{13}$$

When $\boldsymbol{A}$ is not invertible, we can still obtain an equalizer using the Moore-Penrose pseudo-inverse of A. In this case, there would be some residual mismatch-induced interference at the equalizer output which would lead to an error floor. In all of our numerical experiments, we have found that $\boldsymbol{A}$ is invertible, in which case perfect zero-forcing equalization is possible. While we have not been able to find general analytical conditions for invertibility, we provide insight into what such conditions might look like by considering the special case in which the I and Q channel TI-ADCs have the same mismatch parameters; that is, $\boldsymbol{\Delta_I} = \boldsymbol{\Delta_Q}$. In this case, we are able to show (see Appendix A) that the matrix $\boldsymbol{A}$ is invertible as long as the gains are non-zero and the (normalized) timing mismatches have absolute values less than 1. Deriving conditions for the more general scenario of $\boldsymbol{\Delta_I} \neq \boldsymbol{\Delta_Q}$ is left as an open problem.

The complexity of the zero-forcing solution in (13) depends on the number of non-zero entries in $\boldsymbol{A}^{-1}$ which, in general, can be as large as $4M^2$. This results in $4M^2$ real multiplications, which can be excessive for large M. Fortunately, the complexity (in terms of the number of real multiplications) is significantly smaller when the number of interleaved ADCs, L, divides the number of OFDM subcarriers M, as discussed next.

A. Interference structure when L divides M

When L divides M, we prove in the Appendix B that the set $\{0, \cdots, 2M\text{-}1\}$, which can be used to index the rows (columns) of A, can be partitioned into disjoint groups such that $A(k, y)$ is non-zero only when the row and column indices, k and y, belong to the same group. Hence, we can divide the system in (11) into parallel systems of interfering constellation symbols. Also, we observe from (25) that whenever the parallel system contains the real part of the constellation symbol encoded on a particular subcarrier, it also contains the corresponding imaginary part. We refer to these groups of subcarriers as "interference groups." Equalization is performed separately for each interference group. We show that the total complexity, summed over all interference groups is bounded by $8ML$ or equivalently, the average complexity per sample is less than $4L$ real-valued multiplications. When $L \ll M$, this is a significant reduction in complexity, since in general, the average complexity can be as high as $2M$ real-valued multiplications per sample. Thus, it makes sense to restrict attention to the special case when L divides M in system design. We note that the complexity of our interference suppression scheme does not scale up with the desired resolution, and is fixed at $4L$ real-valued multiplications per sample. We return to this observation in Section VI, where we provide explicit comparisons with other available options.

B. Noise Enhancement

In order to obtain an understanding of the noise enhancement caused by our linear interference suppression scheme, we first derive the approximate structure for the noise in (5) after it is sampled at Nyquist rate using the I and Q TI-ADCs. The bandlimited noise process in (5) can be represented as a "sinc" function interpolation (in a mean-squared sense) of its Nyquist rate samples [31]. We then consider the timelimited noise waveform within the OFDM frame interval of $[0, (M-1)T]$, and approximate it as an interpolation of samples within that window (neglecting edge effects, assuming large frame sizes). This yields

$$n(t) \approx \sum_{m=0}^{M-1} n[m]\text{sinc}(t - mT), \qquad t \in [0, (M-1)T] \tag{14}$$

Now, we replace the time-domain noise samples, $\{n[m]\}$, in (14) by their (energy-preserving) FFT coefficients, $\{N[y]\}$, to obtain

$$n(t) \approx \frac{1}{\sqrt{M}} \sum_{y=0}^{M-1} N[y] \sum_{m=0}^{M-1} \text{sinc}(t - mT) e^{\frac{j2\pi ym}{M}} \quad (15)$$

Since the noise samples $\{n[m] = n(mT)\}$ are zero-mean, i.i.d complex Gaussian random variables, $\{N[y]\}$ also have the same statistics. Assuming small side-lobes for the "sinc" function, we can approximate the summation over m given in (15) by an infinite summation, which in turn can be simplified using the Poisson's summation formula,

$$n(t) \approx \sum_{y=0}^{M-1} N[y]\phi_y(t) \quad (16)$$

where $\phi_y(t) = \frac{1}{\sqrt{M}} e^{\frac{j2\pi yt}{MT}}$. Substituting (16) into the received signal model (5), we obtain

$$r(t) = \sum_{y=0}^{M-1} \left(H[y]B[y] + N[y]\right) \phi_y(t) \quad (17)$$

Noting the similarity in the structure of (17) and (5), it can be shown that the frequency-domain model (10) holds even when thermal noise is added at the ADC input, but with $S[y] = H[y]B[y] + N[y]$. When we assume perfect knowledge of the mismatch parameters, this implies that the presence of noise does not degrade the estimates of $\boldsymbol{S}$, or equivalently there is no noise enhancement for the proposed zero-forcing equalizer. Although this claim is obtained as an approximation, the simulation results presented in Section VI, which do not use the approximations in (14) and (16), are consistent with the claim, since they show only a small degradation from the performance without mismatch.

V. Joint Mismatch and Channel Estimation

In this section, we estimate the mismatch parameters jointly with the communication channel parameters by using the channel estimation training sequences. We use the model in (10) to obtain the estimates, and include the effect of thermal noise by taking $S[y] = H[y]B[y] + N[y]$. Since an approximate model is used for the noise samples, the obtained estimates are suboptimal. The channel taps in the frequency domain are correlated (the number of subcarriers, M, is much larger than the number of symbol-rate taps in the time domain channel $N+1$), and neglecting these correlations in frequency domain channel estimation would lead to performance degradation. We therefore adopt the simpler strategy of estimating the channel taps in the time domain. As shown in [32], frequency domain correlations can be easily extracted from such time-domain estimates.

We first rewrite (11) in terms of the time-domain channel taps, denoted by $\tilde{\boldsymbol{h}}$, as follows:

$$\tilde{\boldsymbol{R}} = \boldsymbol{A}(\boldsymbol{D}\tilde{\boldsymbol{h}} + \tilde{\boldsymbol{N}}) + \tilde{\boldsymbol{\Upsilon}} \quad (18)$$

where the matrix $\boldsymbol{D}$, that depends on the training sequence, is given as

$$\boldsymbol{D} = \frac{1}{2} \begin{pmatrix} \text{diag}(\boldsymbol{B}) & \text{diag}(\boldsymbol{B}^*) \\ -j\ \text{diag}(\boldsymbol{B}) & j\ \text{diag}(\boldsymbol{B}^*) \end{pmatrix} \begin{pmatrix} \boldsymbol{F}_{N+1} & j\boldsymbol{F}_{N+1} \\ \boldsymbol{F}^*_{N+1} & -j\boldsymbol{F}^*_{N+1} \end{pmatrix} \quad (19)$$

where $\boldsymbol{F}_{N+1}$ denotes the matrix formed by the first $N+1$ columns of the FFT matrix of size M and "diag($\boldsymbol{B}$)" denotes the diagonal matrix formed by placing all the frequency-domain symbols of the training sequence $\boldsymbol{B}$ along the diagonal.

We observe from (18) that the unknown parameters $\boldsymbol{A}$ (a matrix with $4M^2$ entries) and $\tilde{\boldsymbol{\Upsilon}}$ (a vector with $2M$ entries) actually depend on the mismatch parameters, a collection of $6L$ independent unknowns. In order to obtain an unconditioned problem formulation, we estimate the mismatch parameters instead of the entries of $\boldsymbol{A}$ and $\tilde{\boldsymbol{\Upsilon}}$. Direct joint estimation of the channel taps and the mismatch parameters is complicated, hence we resort to an iterative optimization strategy in which we alternately optimize over the channel taps and the mismatch parameters, while keeping the other fixed. Next, we discuss the alternating steps in the iterative optimization.

A. Channel estimation given mismatch estimates

Given the estimates of $\boldsymbol{A}$ and $\tilde{\boldsymbol{\Upsilon}}$ after the $(k-1)^{\text{th}}$ iteration, denoted by $\boldsymbol{A}^{(k-1)}$ and $\tilde{\boldsymbol{\Upsilon}}^{(k-1)}$, we can use (18) to obtain the least-squares (LS) estimates of the channel taps in the k^{th} iteration,

$$\tilde{\boldsymbol{h}}^{(k)} = (\boldsymbol{D}^H\boldsymbol{D})^{-1}\boldsymbol{D}^H \left(\boldsymbol{A}^{(k-1)}\right)^{-1} (\tilde{\boldsymbol{R}} - \tilde{\boldsymbol{\Upsilon}}^{(k-1)}) \quad (20)$$

where $\boldsymbol{D}^H$ denotes the complex conjugate transpose of $\boldsymbol{D}$. We note that the LS estimates obtained in (20) are also the ML estimates because the noise vector $\tilde{\boldsymbol{N}}$ in (18) has all its entries as independent, Gaussian random variables.

B. Mismatch estimation given channel estimates

For mismatch estimation, we use time-domain samples from (7) because any time-domain sample contains information about the mismatch parameters corresponding to one and only one sub-ADC. Thus, we consider the the samples of the l^{th} sub-ADC of the I-channel, denoted by $\boldsymbol{r}_{I,l}$, to calculate the corresponding mismatch parameters $(g_{I,l}, \delta_{I,l}, \mu_{I,l})$. Using (7)-(9), given the channel estimates at the k^{th} iteration as $\tilde{\boldsymbol{h}}^{(k)}$, we obtain the ML estimates of the gain, timing and voltage offset mismatches as,

$$\begin{aligned}&(g^{(k)}_{I,l}, \delta^{(k)}_{I,l}, \mu^{(k)}_{I,l}) \\ &= \text{argmin}||\boldsymbol{r}_{I,l} - \Re[\boldsymbol{\Delta}_{I,l}(g_{I,l}, \delta_{I,l})\boldsymbol{S}^{(k)}] - \mu_{I,l}||^2 \end{aligned} \quad (21)$$

where $\boldsymbol{\Delta}_{I,l}$, a function of $g_{I,l}$ and $\delta_{I,l}$, represents the matrix formed by the rows of $\boldsymbol{\Delta}_I$ with indices of the form $1+l+dL$ (integer d). In (21), the vector $\boldsymbol{S}^{(k)}$ has entries $H^{(k)}[m]B[m]$. We note that $\boldsymbol{H}^{(k)}$, the estimate (in k^{th} iteration) of the vector of frequency domain channel taps, can be obtained in terms of $\tilde{\boldsymbol{h}}^{(k)}$.

The norm in (21) should ideally take into account the correlation among the noise samples. By considering the standard Euclidean norm, we are implicitly assuming that the noise samples are uncorrelated. This holds when there is no mismatch, but need not be true with mismatch. However, our numerical results in Section VI show that ignoring the noise correlations leads to little degradation in estimation performance for the mismatch levels considered.

TABLE I
SYSTEM PARAMETERS FOR SIMULATIONS AND EXPERIMENTAL PROTOTYPE

Variable (symbol)	Value
OFDM subcarriers (M)	128
Modulation	16-QAM
Channel taps	
Real ($\boldsymbol{h}_I$)	0.5, -1.8 , 1.7, -0.6 , 1.0, 0.2 , 0.4 , -0.6 , 0.3
Imaginary ($\boldsymbol{h}_Q$)	-0.1, -1.8 , 3.8, 1.8 , -0.2, 1.5 , 0.6 , -0.1 , 0.0
Mismatch parameters	
I-component	Relative mismatch in %
Gain ($\boldsymbol{g}_I$)	3.3, -1.4, -9.5, -7.1, 5.7, 9.3, -4.9, 1.1
Timing ($\boldsymbol{\delta}_I$)	4.6, -9.6, -1.3, -0.5, 2.9, 6.9, -0.4, -5.1
Voltage offset ($\boldsymbol{\mu}_I$)	3.6, 5.2, 4.9, -2.2, 3.1, -6.6, 4.1, -9.4

With the Euclidean norm, if we fix the timing mismatch, the objective function in (21) is quadratic in the gain and voltage offset mismatches, hence we can obtain closed-form expressions for the optimal estimates of these mismatch parameters and plug them in. It remains to estimate the timing mismatch parameters, which we do with a one-dimensional numerical search for each sub-ADC. In the latter, we assume that the normalized timing mismatch is bounded to within an interval (e.g., $[-0.1, 0.1]$ corresponds to 10% mismatch).

We perform the optimization in (21) for l in $\{0, \cdots, L-1\}$ to estimate the mismatches for all the sub-ADCs in the I-channel TI-ADC. Exactly the same approach holds for the Q channel as well; the corresponding expressions are obtained by replacing I in (21) with Q.

An important design issue is the number of iterations required. In this paper, we fix the number of iterations. An alternative, data-dependent criterion might be to stop when the change from the prior iteration is "small enough". We do not consider this here, since as few as three iterations are found to work well in the settings we have considered. We also leave as an open problem the issue of whether our iterative algorithm can be proven to converge to a global optimum.

VI. ILLUSTRATIONS

In this section, we consider example scenarios that illustrate the structure of the mismatch-induced interference in an OFDM system. We provide simulation and experimental results to evaluate the performance of our mismatch estimation and compensation schemes. The relevant system parameters are given in Table I. We consider OFDM-based transmission with 128 subcarriers, each of which is modulated by symbols drawn from the 16-QAM constellation. The channel taps are obtained from an instance of CM 1, the LOS channel model defined in the UWB standardization process [28]. In Table I, we give mismatch parameters corresponding to a level of 10%, for a TI-ADC with eight interleaved ADCs. By 10% mismatches, we mean that the values of gain, timing and voltage offset mismatches are chosen uniformly in $[-0.1, 0.1]$, $[-\frac{T_o}{10}, \frac{T_o}{10}]$ and $[-\frac{\mathcal{A}}{10}, \frac{\mathcal{A}}{10}]$ respectively. Here, T_o and $\mathcal{A}$ indicate the sampling period and the root-mean-square (rms) value of the ADC input signal's amplitude. The mismatch parameters given in Table I correspond to the TI-ADC for the I-channel, and we obtain the parameters for the Q-channel TI-ADC by circularly shifting the I-channel parameters by one element. We now provide simulation results to understand the effect, structure and suppression of the mismatch-induced interference.

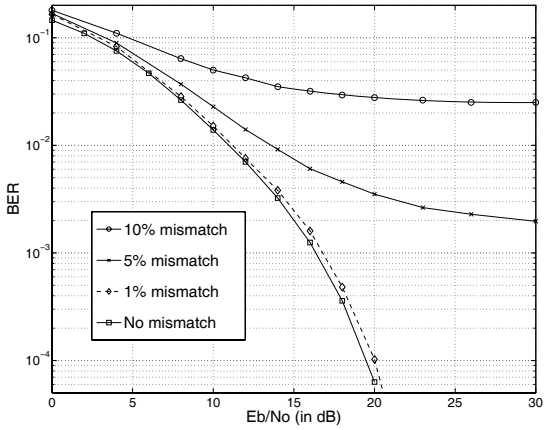

Fig. 4. Effect of mismatches in a TI-ADC (with 8 sub-ADCs) for OFDM transmission employing 16-QAM constellation. Perfect channel knowledge is assumed.

A. Mismatch-induced Error Floors

The signal-dependent interference seen at any subcarrier due to mismatch, left uncorrected, is a sum of scaled versions of the constellation symbols from other subcarriers, modeled as independent random variables. Applying the central limit theorem, we can model the total mismatch-induced interference at any subcarrier as Gaussian, where the mean is determined by the voltage offset mismatches and the variance can be obtained in terms of gain and timing mismatch parameters using (10). This Gaussian approximation is validated by simulation results for the 16-QAM constellation in Fig. 4, where we show the performance for eight interleaved ADCs in three different mismatch settings of 10%, 5% and 1%. For the 1% and 5% mismatch levels, the mismatch parameters are the scaled versions (by 0.1 and 0.5 respectively) of the parameters for the 10% level given in Table I. The analysis predicts an error floor due to mismatch as E_b/N_o gets large, and this is borne out by simulations. For mismatch levels of 10% and 5%, we observe error floors of 10^{-2} and 10^{-3}, respectively. For 1% mismatch, we do not observe an error floor for BER up to 10^{-4}. For a given mismatch level, larger constellations see more severe error floors: while 1% mismatch does not give an error floor for 16-QAM, there is an error floor at 10^{-3} for a 256-QAM constellation.

B. Structure of Mismatch-induced Interference

We consider two settings to illustrate how crucially the structure of the interference depends on whether the number of interleaved sub-ADCs L divides the number of subcarriers M (we have $M = 128$): $L = 6$ (in which L does not divide M) and $L = 8$ (in which L divides M). The mismatch parameters for $L = 6$ are taken as the first 6 entries of the parameters given for $L = 8$ in Table I. Consider the real part of the first subcarrier's constellation symbol as the signal of interest. The SNR without mismatch is fixed at 26 dB, which corresponds to E_b/N_o of 20dB for 16-QAM. From Fig. 5, we observe that

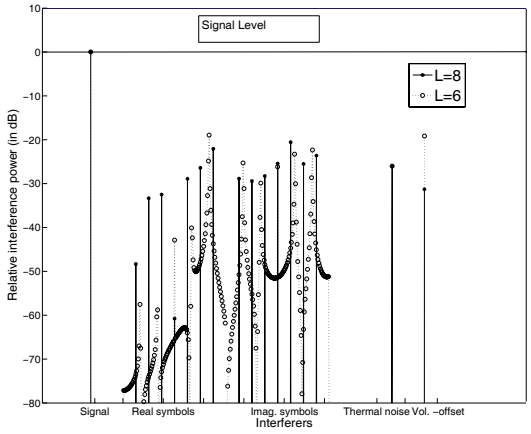

Fig. 5. Structure of mismatch-induced interference: the relative interference for the real part of the constellation symbol of first subcarrier (signal) from all the subcarriers is shown. The signal level is normalized to 0dB, and the values of "L" in the legend indicate the number of sub-ADCs interleaved.

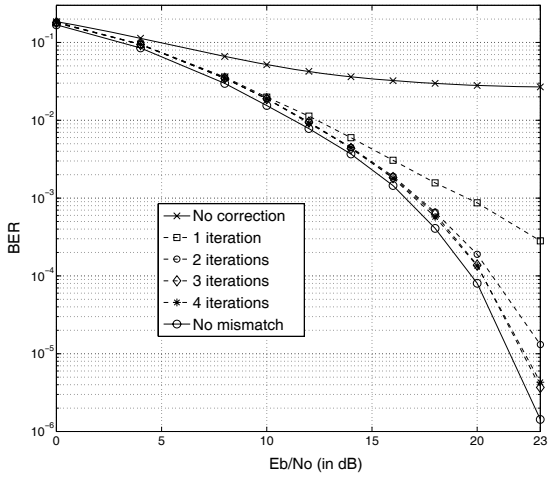

Fig. 6. BER after estimation and correction of 10% mismatches in a TI-ADC (with 8 sub-ADCs) used for OFDM signal reception employing 16 QAM constellation. The number of iterations of the estimation algorithm is shown in the legend.

the gain and timing mismatches are the dominant sources of interference in both settings. For $L = 8$, only constellation symbols corresponding to seven other subcarriers and the imaginary part of the first subcarrier's constellation symbol interfere with the signal of interest. In contrast, for $L = 6$, for which L does not divide M, all other subcarriers interfere with the signal of interest.

C. Suppression of Mismatch-induced interference

We now illustrate the mismatch compensation and estimation algorithms proposed in Sections IV and V for eight interleaved ADCs with a mismatch level of 10%. For training, we use six repetitions of a Pseudo Noise (PN) sequence with 128 QPSK symbols, which was originally proposed for channel estimation during the UWB standardization process [28].

Fig. 6 shows that the BER falls rapidly with an increasing number of iterations, and that we can obtain performance comparable to that without mismatch in only three iterations. The proposed mismatch compensation scheme has a complexity of 32 real-valued multiplications per sample.

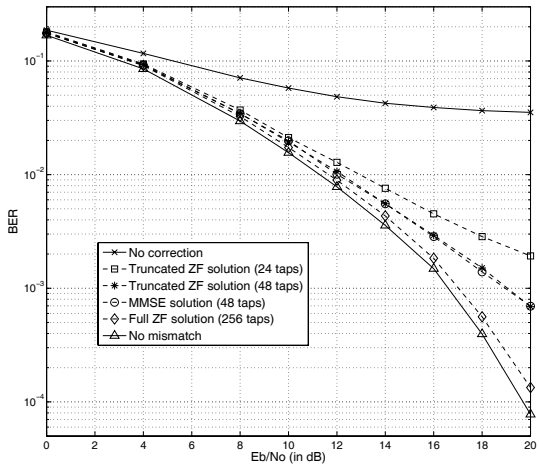

Fig. 7. BER after estimation and correction of 10% mismatches in a TI-ADC (with L=6 sub-ADCs) used for OFDM signal reception employing 16 QAM constellation. The complexity (in terms of number of real-valued multiplications per sample) is indicated in the legend and the number of iterations of the estimation algorithm is fixed at 3.

In Fig. 7, we show the performance of the proposed algorithms for a TI-ADC with $L = 6$ sub-ADCs. From the discussion in Section IV-A, the complexity can be as large as $2M = 256$ real-valued multiplications per sample. Fig. 7 illustrates the performance for the 256-tap, zero-forcing equalizer, as well as for suboptimal equalizers with fewer taps, chosen by keeping coefficients of the zero-forcing equalizer with large absolute values. We refer to these sub-optimal equalizers as *truncated* zero-forcing equalizers. While the full-complexity equalizer does eliminate mismatch-induced interference, sub-optimal equalizers with fewer than 256 taps incur error floors due to residual interference. We also optimized the coefficients of the sub-optimal equalizer (with 48 taps) for minimizing the residual interference power using the MMSE criterion, but obtained an insignificant performance improvement. We conclude that L dividing M is a superior design choice from the point of view of performance-complexity tradeoffs.

D. Experimental results using hardware TI-ADC prototype

The results from computer simulation are supplemented with experimental results from a hardware prototype, which is obtained by modifying the experimental set-up in [15] to handle communication signals. The prototype, shown in Fig. 8, employs a TI-ADC sampling at 400MSa/s, assembled by interleaving four commercially available ADCs from Analog Devices, Inc., each sampling at 100 MSa/s with 14 bits of resolution. We note the low sampling rate of the prototype (compared to GHz sampling rates required for the multi-Gigabit systems in [28], [29]), chosen on account of the ease of availability of the commercial ICs, and we refer the reader to [6], [7], where TI-ADCs with GHz sampling rates are realized. A 100MHz clock, after bandpass filtering to eliminate wide-band white noise, feeds a clock distribution board that provides

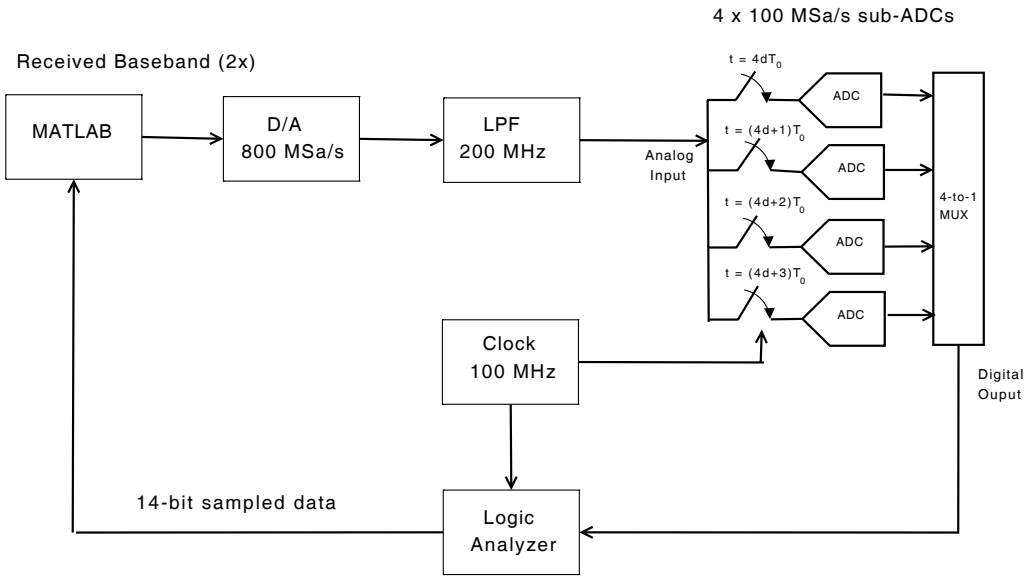

Fig. 8. TI-ADC experimental prototype with four interleaved ADCs. D/A and LPF refer to digital-to-analog converter and low pass filter respectively. We assume that $T_o = 2.5$ns and that d takes integral values.

timing for the interleaved ADCs. The distribution board uses a 1-to-4 power splitter and delay lines to create four 100MHz clocks with nominal phase offsets of $0^o, 90^o, 180^o$ and 270^o. Each clock path has a voltage-controlled phase shifter using a varactor. For our experiments, however, this fine-tuning knob is disabled. Sampling time mismatches of the prototype TI-ADC are mainly due to relative phase errors in the 1-to-4 power splitter and the voltage-controlled phase shifters.

We now explain the signal flow through the prototype. We assume the baseband signal to be limited to $[-200, 200]$ MHz. The digital version of the received (baseband) signal, for both the I and Q channels, is generated using MATLAB at twice the Nyquist rate (800 MSamples/sec). The signals corresponding to the I and Q channels are separated by a fixed white space so that they can be sampled by the same TI-ADC; the data for the individual channels can then be obtained by de-serializing the TI-ADC output. Using an Arbitrary Waveform Generator (AWG520 from Sony/Tektronix) as a D/A converter, the MATLAB output is converted into an analog signal. The signal is then lowpass filtered to 200 MHz and fed to the TI-ADC. The Nyquist sampled (400 Msamples/sec) digital output from the ADC is collected at the Logic Analyzer (Tektronix), which has a routine for subtracting the running-average mean from the sub-ADC output to eliminate voltage offsets. We can therefore ignore voltage offset mismatch. We use MATLAB to process the data obtained from the Logic Analyzer.

Using the joint estimation algorithm of Section V, we obtained gain mismatch estimates of $\{0.19, 0.08, 0.40, 0.25\}\%$ and timing mismatch estimates of $\{-8.0, 5.0, -5.7, 8.5\}\%$. We note that these parameters correspond to both I and Q channels since the same TI-ADC is used to sample both channels. We can compare the complexity of the proposed scheme with a standard time-domain compensation scheme in [15], where four sub-ADCs are interleaved and only the I-channel is present. The scheme in [15] uses 21 multiplications per sample for a required resolution of 14 bits, while the proposed scheme, independent of the required resolution, has a significantly smaller complexity of 8 multiplications per sample[1].

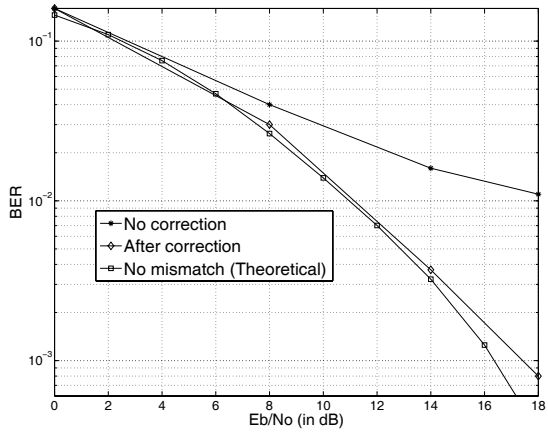

Fig. 9. Experimental results from the prototype confirm the efficacy of the proposed mismatch estimation and equalization scheme.

Fig. 9 depicts the BER performance. We observe an error floor when the mismatches are left uncorrected, but we obtain a performance close to that without mismatch after zero-forcing equalization, thus verifying the efficacy of the proposed algorithms in a realistic setting. For the Spurious-Free-Dynamic-Range (SFDR) or the Effective-Number-Of-Bits (ENOB) metrics, we refer the reader to [15], where the same experimental set-up is used for realizing a general-purpose TI-ADC.

VII. Conclusions

The results in this paper demonstrate that low-complexity frequency-domain equalization strategy is a promising

[1]The complexity of the proposed scheme is smaller than the upper bound (of $4L = 16$ multiplications/sample) given in Section IV-A, because the I and Q channel TI-ADCs have the same mismatch parameters in the experimental set-up.

approach for joint mismatch compensation and demodulation in multiGigabit OFDM systems. The approach is most effective when the number of sub-ADCs is moderate, and gives the best performance-complexity tradeoff when the number of sub-ADCs divides the number of subcarriers. Potential applications include analog-to-digital conversion at Gigahertz rates or higher, prior to baseband digital signal processing in multiGigabit transceivers for emerging applications in UWB and millimeter wave communication.

There are a number of open issues that deserve further investigation. We would like to determine whether the iterative algorithm for joint mismatch and channel estimation is guaranteed to converge to a good (or, even better, an optimal) solution. It would be useful to devise low-complexity techniques for updating the mismatch estimates (rather than estimate them afresh for each packet). Finally, a fundamental issue is the design of alternative mismatch compensation schemes that scale well as the number of sub-ADCs becomes large (the complexity of the proposed frequency-domain equalization scheme, which scales linearly with the number of sub-ADCs, may become prohibitive in this regime).

APPENDIX A
INVERTIBILITY OF $\boldsymbol{A}$

From the definition in (12), $\boldsymbol{A}$ is invertible whenever $\tilde{\boldsymbol{F}}$ and $\tilde{\boldsymbol{\Delta}}$ are invertible. Clearly, $\tilde{\boldsymbol{F}}$ is invertible; this is because, whenever $\tilde{\boldsymbol{F}}\tilde{\boldsymbol{x}} = 0$, it implies that $\boldsymbol{F}\boldsymbol{x} = 0$, and hence we can extend the invertibility of $\boldsymbol{F}$ to $\tilde{\boldsymbol{F}}$. We now assume that $\boldsymbol{\Delta}_I = \boldsymbol{\Delta}_Q = \boldsymbol{\Delta}$, when we have $\tilde{\boldsymbol{\Delta}}\tilde{\boldsymbol{x}} = \boldsymbol{\Delta}\boldsymbol{x}$, and hence $\tilde{\boldsymbol{\Delta}}$ is invertible whenever $\boldsymbol{\Delta}$ is invertible. Using (9), we can write $\boldsymbol{\Delta}$ as a product of a diagonal matrix $\boldsymbol{D}_{\boldsymbol{\Delta}}$ and a Vandermonde-matrix $\boldsymbol{V}_{\boldsymbol{\Delta}}$, which are defined as,

$$\begin{aligned} \boldsymbol{D}_{\boldsymbol{\Delta}}(m,m) &= 1+g_m; \quad \boldsymbol{D}_{\boldsymbol{\Delta}}(m,y) = 0, \text{ for } m \neq y; \\ \boldsymbol{V}_{\boldsymbol{\Delta}}(m,y) &= e^{\frac{j2\pi y}{M}(m+\delta_m)}, \end{aligned} \tag{22}$$

where m and y take integral values between 0 and $M-1$, and where we dispense with the subscripts I and Q, since $\boldsymbol{\Delta}_I = \boldsymbol{\Delta}_Q$. The diagonal matrix $\boldsymbol{D}_{\boldsymbol{\Delta}}$ is invertible when all of its diagonal elements $1+g_m$, which correspond to the sub-ADC gains, are non-zero. The Vandermonde matrix $\boldsymbol{V}_{\boldsymbol{\Delta}}$ is invertible when all its parameters $\{e^{\frac{j2\pi}{M}(m+\delta_m)}\}$ are distinct. Clearly, when m varies over integer values between 0 and $M-1$, the Vandermonde parameters are all distinct, as long as $|\delta_m| < 1$ for all m (i.e., the normalized timing mismatches are bounded by one). Under these conditions, therefore, the matrix $\boldsymbol{A}$ is invertible.

APPENDIX B
STRUCTURE OF THE MATRIX $\boldsymbol{A}$ WHEN L DIVIDES M

We first consider the structure of the matrix $\boldsymbol{F}\boldsymbol{\Delta}_I$ when L divides M. We write the $(k,y)^{\text{th}}$ element of the matrix $\boldsymbol{F}\boldsymbol{\Delta}_I$ as follows:

$$(\boldsymbol{F}\boldsymbol{\Delta}_I)_{(k,y)} = \frac{1}{M}\sum_{l=0}^{L-1}(1+g_{I,l})e^{j2\pi y\delta_{I,l}/M}\sum_{m\in M_l} e^{-j2\pi m(k-y)/M} \tag{23}$$

where M_l denotes the set of all m for which $m \bmod L = l$. Evaluating the summation over m in (23), we have that $(\boldsymbol{F}\boldsymbol{\Delta}_I)_{(k,y)}$ is non-zero only for a set of L indices $y \in \mathcal{Y}_k$ where $\mathcal{Y}_k$ is given by

$$\mathcal{Y}_k = \{y : 0 \leq y \leq M-1, y \bmod (M/L) = k\} \tag{24}$$

From (24), we observe that $\mathcal{Y}_y = \mathcal{Y}_k$ for any integer $y \in \mathcal{Y}_k$. This readily implies that the set of indices $\xi = \{0,\cdots,M-1\}$ can be partitioned into M/L disjoint groups, which are the sets $\mathcal{Y}_k$ for $k = \{0,\cdots,\frac{M}{L}-1\}$, such that $(\boldsymbol{F}\boldsymbol{\Delta}_I)_{(k,y)}$ is nonzero only when k and y belong to the same group. Since no information about the exact mismatch parameters is utilized during the proof, the result directly extends for the matrix $\boldsymbol{F}\boldsymbol{\Delta}_Q$. We can repeat the analysis between (23)-(24) for the matrix $\boldsymbol{F}^*\boldsymbol{\Delta}_I$ to understand that its $(k,y)^{\text{th}}$ element is non-zero only when $y \in \mathcal{Y}_{-k}$.

Now, we understand that all the $M \times M$ sub-matrices of $\boldsymbol{A}$, that appear in the definition of $\boldsymbol{A}$ given in (12), can be written in terms of $\boldsymbol{F}\boldsymbol{\Delta}_I$, $\boldsymbol{F}^*\boldsymbol{\Delta}_I$ and their conjugates $\boldsymbol{F}^*\boldsymbol{\Delta}_I^*$ and $\boldsymbol{F}\boldsymbol{\Delta}_I^*$. Hence, we extend the results derived for the structure of these matrices to infer that the index set $\{0,\cdots,2M-1\}$ can be partitioned into disjoint groups such that $\boldsymbol{A}(k,y)$ is non-zero only when k and y belong to the same group. When M/L is even, the disjoint groups can be obtained as

$$G_k = \begin{cases} \mathcal{Y}_k \cup \mathcal{Y}_{-k} \cup (M+\mathcal{Y}_k) \cup (M+\mathcal{Y}_{-k}), & 1 \leq k \leq \frac{M}{2L}-1 \\ \mathcal{Y}_k \cup (M+\mathcal{Y}_k), & k \in \{0, \frac{M}{2L}\} \end{cases} \tag{25}$$

where $M+X$ denotes the addition of M to all the elements of the set X. From (25), we have two groups of size $2L$ and $\left(\frac{M}{2L}-1\right)$ groups of size $4L$. The complexity of zero-forcing equalization, given in (13), for a group of size X is at most X^2. Hence, we can obtain the total complexity to be at most $8ML-8L^2$. We can perform a similar analysis for odd M/L to obtain an equalization complexity of $8ML-4L^2$.

ACKNOWLEDGMENT

The authors would like to thank Dr. Jaspreet Singh, Sriram Venkateswaran, Prof. Shiv Chandrasekharan and Prof. James Buckwalter for the valuable technical discussions. They also thank anonymous reviewers for their detailed and insightful comments.

REFERENCES

[1] S. Adee, "The data: 37 years of Moore's Law," *IEEE Spectrum*, vol. 45, May 2008.
[2] B. Le, T. W. Rondeau, J. H. Reed, and C. W. Bostian, "Analog-to-digital converters," *IEEE Signal Process. Mag.*, vol. 22, Nov. 2005.
[3] J. Craninckx and G. V. Plas, "A 65J/conversion-step 0-to-50MS/s, 0-to-0.7mW, 9b charge-sharing SAR ADC in 90nm digital CMOS," *IEEE International Solid State Circuits Conf. (ISSCC)*, 2007.
[4] J. Hu, N. Dolev, and B. Murmann, "A 9.4-bit, 50-MS/s, 1.44-mW pipelined ADC using dynamic residue amplification," *IEEE J. Solid State Circuits*, vol. 42, Dec. 2007.
[5] C. Vogel and H. Johansson, "Time-interleaved analog-to-digital converters: status and future directions," *Proc. IEEE Intl. Symp. Circuits Syst. (ISCAS)*, May 2006.
[6] B. P. Ginsburg and A. P. Chandrakasan, "Highly interleaved 5-bit, 250-MSample/s, 1.2-mW ADC with redundant channels in 65-nm CMOS," *IEEE J. Solid State Circuits*, vol. 43, Dec. 2008.
[7] S. K. Gupta, M. A. Inerfield, and J. Wang, "A 1-GS/s 11-bit ADC with 55-dB SNDR, 250-mW power realized by a high bandwidth scalable time-interleaved architecture," *IEEE J. Solid State Circuits*, vol. 41, pp. 2650-2657, Dec. 2006.

[8] S. M. Louwsma, A. J. M. V. Tuijl, M. Vertregt and B. Nauta, " A 1.35 GS/s, 10 b, 175 mW time-interleaved A/D converter in 0.13 μm CMOS," *IEEE J. Solid State Circuits*, vol. 43, Apr. 2008.

[9] A. Varzaghani and C. K. K. Yang, "A 4.8 GS/s 5-bit ADC-based receiver with embedded DFE for signal equalization," *IEEE J. Solid State Circuits*, vol. 44, Mar. 2009.

[10] C. C. Hsu, F. C. Huang, C. Y. Shih, C. C. Huang, Y. H. Lin, C. C. Lee, and B. Razavi, "An 11b 800MS/s time-interleaved ADC with digital background calibration," *IEEE International Solid State Circuits Conf. (ISSCC)*, 2007.

[11] J. Elbornsson, F. Gustafsson, and J. E. Eklund, "Analysis of mismatch effects in a randomly interleaved A/D converter system," *IEEE Trans. Circuits Syst.*, vol. 52, Mar. 2005.

[12] P. Satarzadeh, B. C. Levy, P. J. Hurst, "Bandwidth mismatch correction for a two-channel time-interleaved A/D converter," *IEEE International Symp. Circuits Syst. (ISCAS)*, 2007.

[13] D. Camarero, K. B. Kalaia, J. F. Naviner, and P. Loumeau, "Mixed-signal clock-skew calibration technique for time-interleaved ADCs," *IEEE Trans. Circuits Syst. - I*, vol. 55, Dec. 2008.

[14] A. Haftbaradaran and K. W. Martin, "A background sample-time error calibration technique using random data for wide-band high-resolution time-interleaved ADCs," *IEEE Trans. Circuits Syst.-II*, vol. 55, Mar. 2008.

[15] M. Seo, M. J. W. Rodwell, and U. Madhow, "Comprehensive digital correction of mismatch errors for a 400-msamples/s 80-dB SFDR time-interleaved analog-to-digital converter," *IEEE Trans. Microwave Theory Techniques*, vol. 53, pp. 1072-1082, Mar. 2005.

[16] H. Johansson and P. Lowenborg, "Reconstruction of non-uniformly sampled bandlimited signals by means of digital fractional delay filters," *IEEE Trans. Signal Process.*, vol. 50, no. 11, pp. 2757- 2767, Nov. 2002.

[17] M. Seo, M. J. W. Rodwell, and U. Madhow, "Generalized blind mismatch correction for two-channel time-interleaved A/D converters," *IEEE International Conf. Acoustics, Speech, Signal Process. (ICASSP)*, 2007.

[18] S. Huang and B. C. Levy, "Blind calibration of timing offsets for four-channel time-interleaved ADCs," *IEEE Trans. Circuits Syst.*, vol. 54, pp. 863-876, Apr. 2007.

[19] J. Elbornsson, F. Gustafsson, and J. E. Eklund, "Blind equalization of time errors in a time-interleaved ADC system," *IEEE Trans. Signal Process.*, vol. 53, Apr. 2005.

[20] T. Strohmer and J. Tanner, "Fast reconstruction methods for bandlimited functions from periodic non-uniform sampling," *Siam J. Numerical Analysis*, vol. 44, pp. 1073-1094, 2006.

[21] R. S. Prendergast, B. C. Levy, and P. J. Hurst, "Reconstruction of band-limited periodic non-uniformly sampled signals through multi-rate filter banks," *IEEE Trans. Circuits Syst.-I*, vol. 51, pp. 1612-1622, Aug. 2004.

[22] Y. C. Eldar and A. V. Oppenheim, "Filterbank reconstruction of bandlimited signals from nonuniform and generalized samples," *IEEE Trans. Signal Process.*, vol. 48, Oct. 2000.

[23] D. Marelli, K. Mahata, and M. Fu, "Linear LMS compensation for timing mismatch in time-interleaved ADCs," *IEEE Industrial Electron. Conf. (IECON)*, 2008.

[24] Y. Oh and B. Murmann, "System embedded ADC calibration for OFDM receivers," *IEEE Trans. Circuits Syst.-I*, vol. 53, Aug. 2006.

[25] M. Soudan and R. Farrell, "Impact of time-interleaved analog-to-digital converter mismatch on digital receivers," *IEEE International Conf. Electron., Circuits Syst. (ICECS)*, 2008.

[26] J. Singh, O. Dabeer, and U. Madhow, "On the limits of communication with low-precision analog-to-digital conversion at the receiver," *IEEE Trans. Commun.*, vol. 57, Dec. 2009.

[27] J. Singh, P. Sandeep, and U. Madhow, "Multi-gigabit communication: the ADC bottleneck," in *Proc. 2009 IEEE International Conf. Ultra-Wideband (ICUWB)*, Sep. 2009.

[28] IEEE 802.15 WPAN High rate Alternative PHY Task Group 3a. [Online]. Available: http://www.ieee802.org/15/pub/TG3a.html

[29] IEEE 802.15 WPAN High rate Alternative PHY Task Group 3c. [Online]. Avalable: http://www.ieee802.org/15/pub/TG3c.html

[30] U. Madhow, *Fundamentals of Digital Communication*. Cambridge, 2008.

[31] A. J. Jerri, "The Shannon sampling theorem—its various extensions and application: a tutorial review," in *Proc. IEEE*, vol. 65, Nov. 1977.

[32] L. Deneire, P. Vandenameele, L. v. d. Perre, B. Gyselinckx, and M. Engels, "A low-complexity ML channel estimator for OFDM," *IEEE Trans. Commun.*, vol. 51, Feb. 2003.

Sandeep Ponnuru received his bachelor's degree in electrical engineering from the Indian Institute of Technology, Kanpur, in 2006. Since then, he has been a doctoral student in the Electrical and Computer Engineering department at the University of California, Santa Barbara (UCSB). His research at UCSB focuses on the use of time-interleaved analog-to-digital converters in communication systems.

Munkyo Seo received the B.S.E.E. and M.S.E.E. degrees in electronic engineering from Seoul National University, Seoul, Korea, in 1994 and 1996, respectively, and the Ph.D. degree in electrical engineering from the University of California, Santa Barbara (UCSB), in 2007. From 1997 to 2002, he was a Research Engineer with LG Electronics Inc., designing RF and microwave subsystems for wireless communication. He was an Assistant Project Scientist with UCSB from 2008 to 2009. His research at UCSB focused on signal processing techniques for time-interleaved analog-to-digital converters, novel communication/sensor network systems, and millimeter-wave integrated circuits in nanoscale CMOS and HBT technologies. In 2009, he joined Teledyne Scientific Company (formerly, Rockwell Scientific Company), Thousand Oaks, CA, where he is now working on the design of high-resolution mixed-signal circuits and millimeter-wave circuits operating beyond 300 GHz. Dr. Seo won the 2008 UCSB Lancaster Dissertation Award for his dissertation in the area of Mathematics, Physical Sciences, and Engineering. He also received an Honorary Mention in the Student Paper Competition of 2008 IEEE MTT-S International Microwave Symposium for his work on distributed phased array techniques for energy-efficient wireless sensor networks.

Upamanyu Madhow received his bachelor's degree in electrical engineering from the Indian Institute of Technology, Kanpur, in 1985. He received the M. S. and Ph. D. degrees in electrical engineering from the University of Illinois, Urbana-Champaign in 1987 and 1990, respectively. From 1990 to 1991, he was a Visiting Assistant Professor at the University of Illinois. From 1991 to 1994, he was a research scientist at Bell Communications Research, Morristown, NJ. From 1994 to 1999, he was on the faculty of the Department of Electrical and Computer Engineering at the University of Illinois, Urbana- Champaign. Since December 1999, he has been with the Department of Electrical and Computer Engineering at the University of California, Santa Barbara, where he is currently a Professor. His research interests are in communication systems and networking, with current emphasis on wireless communication, sensor networks and multimedia security. Dr. Madhow is a recipient of the NSF CAREER award. He has served as Associate Editor for the IEEE TRANSACTIONS ON COMMUNICATIONS, IEEE TRANSACTIONS ON INFORMATION THEORY, and textscIEEE Transactions on Information Forensics and Security. He is the author of the graduate textbook, *Fundamentals of Digital Communication*, published by Cambridge University Press.

Mark Rodwell (B.S., University of Tennessee, Knoxville, 1980, M.S. Stanford University 1982, Ph.D. Stanford University 1988) is Professor and Director of the UCSB Nanofabrication Laboratory and NSF Nanofabrication Infrastructure Network (NNIN), and the SRC Non-classical CMOS Research Center at the University of California, Santa Barbara. He was at AT&T Bell Laboratories, Whippany, N.J. during 1982-1984. Prof. Rodwell received the 2010 IEEE Sarnoff Award and the 2009 IEEE IPRM Conference Award for the development of InP-based bipolar IC technology, at both device and circuit design level, for mm-wave and sub-mm-wave applications. His group's work on GaAs Schottky-diode ICs for sub-picosecond / mm-wave instrumentation was awarded the 1997 IEEE Microwave Prize and the 1998 European Microwave Conference Microwave Prize. Prof. Rodwell was elected IEEE Fellow in 2003.